Quantitative Investigation of Room-Temperature Breakdown Effects in Pixelated TlBr Detectors

Will Koehler, Zhong He, *Senior Member, IEEE*, Crystal Thrall, Sean O'Neal, Hadong Kim, Leonard Cirignano, and Kanai Shah

***Abstract*—Due to favorable material properties such as high atomic number (Tl: 81, Br: 35), high density (7.56 g/cm^3), and a wide band gap (2.68 eV), thallium-bromide (TlBr) is currently under investigation for use as an alternative room-temperature semiconductor gamma-ray spectrometer. TlBr detectors can achieve less than 1% FWHM energy resolution at 662 keV, but these results are limited to stable operation at $-20°$C. After days to months of room-temperature operation, ionic conduction causes these devices to fail. This work correlates the varying leakage current with alpha-particle and gamma-ray spectroscopic performances at various operating temperatures. Depth-dependent photopeak centroids exhibit time-dependent transient behavior, which indicates trapping sites form near the anode surface during room-temperature operation. After refabrication, similar performance and functionality of failed detectors returned.**

***Index Terms*—Alternative room temperature semiconductor, TlBr spectrometers.**

I. Introduction

HAVING a high density and atomic number, thallium-bromide (TlBr) is a highly efficient and therefore desired material for gamma-ray spectroscopy. Additionally, TlBr has a relatively wide bandgap (2.7 eV), making it operable at room temperature with low thermal noise [1]. Unlike other room-temperature semiconductors currently under investigation (e.g. CdZnTe), TlBr has a simple cubic crystal structure and a melting point at $480°$C, which simplifies the growing process.

While long-term stability has been achieved at $-20°$C, TlBr detectors break down, or polarize, after days to months of room-temperature operation [1]–[6]. It has been hypothesized that breakdown at room temperature is the result of ionic conduction, wherein space charge collects under the electrodes and reduces the effective electric field [7], [8]. Eventually, the field is not strong enough to collect the charges before significant trapping occurs, and the device fails. Alternative work concludes that the ultimate failure of the device is caused by the migration of the electrode metals into the crystal bulk, creating sub-gap traps [5].

Reports have shown stable room-temperature operation by applying Tl electrodes [7] and periodically switching the polarity of the applied bias [9]. Tl is extremely toxic, severely complicating the electrode fabrication process. Periodically switching the polarity is undesirable with pixelated detectors in which the anode must be the pixelated electrode for optimal signal generation.

Each TlBr detector tested at the University of Michigan (UM) demonstrated unique behavior. Detectors have completely failed after hours to months of room-temperature operation (the term "polarization" is used to describe this failure mechanism) [10]. In this work, complete failure refers to cathode or anode breakdown in which the leakage current saturates the preamplifier. In some detectors, the cathode signals demonstrated breakdown behavior while the anode signals remained stable. However, both the anode and cathode signals demonstrated breakdown behavior in other detectors. Additionally, the time-dependent gamma-ray spectroscopy performance varied greatly between detectors.

In an effort to quantify the polarization process, the material properties (leakage current and electron drift velocity) and detector properties (signal amplitude gain shift and energy resolution) were monitored during room-temperature operation. The experimental results isolate the degradation effects to within about 0.5 mm of the anode surface. As a result, two failed detectors were refabricated after 0.5 mm of material was removed near both electrode surfaces. It was necessary to remove material near the cathode to ensure that the entire cathode surface was removed and to properly etch the surface before the new electrode was applied.

A. Experimental Setup

The TlBr detectors tested in this work were approximately 5 mm in each dimension (thicknesses ranged from 4 mm to 5.68 mm) and were fabricated by Radiation Monitoring Devices, Inc. Each detector had a three-by-three pixelated anode and a planar cathode. The pixels were 0.9 mm x 0.9 mm and had a 1 mm pixel-pitch. The crystals were grown via the traveling zone method and an evaporator was used to apply Cr/Au contacts. The signals from the nine anodes and single cathode were read out using eV-Products 509 charge sensitive preamplifiers, whose outputs were digitized by a computer-operated 14-bit GaGe Octopus CompuScope. Each of the ten waveforms was recorded in 512 data points sampled every 100 ns. All ten signals

Manuscript received December 02, 2013; revised April 24, 2014; accepted August 09, 2014. Date of publication September 12, 2014; date of current version October 09, 2014. This work was supported by DHS DNDO (SBIR contract HSHQDC-12-C-00107) through RMD and DOE (Award DE-AC52-07NA27344) through LLNL.

W. Koehler, Z. He, C. Thrall, and S. O'Neal are with the Department of Nuclear Engineering and Radiological Sciences, University of Michigan, Ann Arbor, MI 48109 USA (e-mail: koehlerw@umich.edu).

H. Kim, L. Cirignano, and K. Shah are with Radiation Monitoring Devices Inc., Watertown, MA 02472 USA.

Color versions of one or more of the figures in this paper are available online at http://ieeexplore.ieee.org.

Digital Object Identifier 10.1109/TNS.2014.2348535

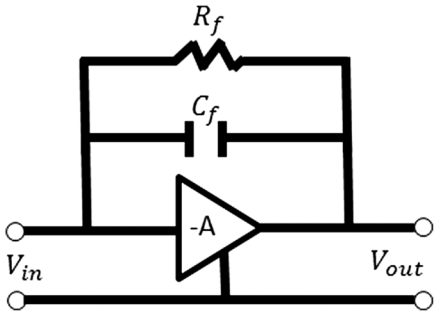

Fig. 1. Simplified schematic for an eV-Products preamplifier. The bulk leakage current must got through the feedback resistor, R_f, which has a measured value of $(9.71 \pm 0.22) \times 10^8\ \Omega$.

were recorded when the amplitude of any anode signal crossed a threshold and triggered the system. To ensure precise temperatures, the measurements were performed in a Thermotron S-1.2-3200 environmental chamber with less than $0.1°\mathrm{C}$ variation. Room-temperature measurements were also performed in the environmental chamber to maintain a constant $20°\mathrm{C}$ temperature. All detectors were cathode biased to -1000 V and flood irradiated with $^{137}\mathrm{Cs}$ for gamma measurements. Alpha measurements were performed by irradiating the cathode side with an $^{241}\mathrm{Am}$ source. Alpha data are not available for all pixels due to geometric limitations.

B. Leakage Current Measurements

From the simplified schematic in Fig. 1, leakage currents were calculated for each pixel by measuring the DC offset of the preamplifier output signal. The bulk leakage current in the detector must pass through the feedback resistor, the only DC path. Using Ohms Law, $I_{leak} = V_{DC}/R_f$, where I_{leak} is the leakage current, V_{DC} is the measured DC offset at the output of the preamplifier, and R_f is the value of the feedback resistor, measured to be $(9.71 \pm 0.22) \times 10^8\ \Omega$. The cathode preamplifier was AC coupled, therefore this method only worked on the pixelated anodes.

II. Methods

A. Gamma-Ray Data Analysis

Due to the small active volume of the detectors, gamma-ray measurements were analyzed in twenty-four-hour data sets. Only single-pixel events were analyzed. The anode waveforms were shaped using a digital CR-$(\mathrm{RC})^4$ shaper with a shaping time of $15\ \mu$s, and the gamma spectra were corrected for electron trapping and weighting potential effects (both of which are depth-dependent), using the cathode-to-anode signal ratio (CAR) [11].

B. Alpha-Particle Data Analysis

Due to their short mean free path, alpha-particles generate electron clouds very near the cathode surface. The alpha-particle-induced electron clouds then drift through the entire detector bulk. Because of the linear cathode weighting potential, a change in cathode waveform amplitude is proportional to a change in depth. The depth-dependent drift velocity was calculated by dividing the change in cathode signal amplitude by the change in time for each of forty cathode-signal depth bins. Pulse amplitude and peaking time filters were used to discriminate gamma-ray and pileup events. These techniques have previously been applied to TlBr and CdZnTe detectors [12], [13].

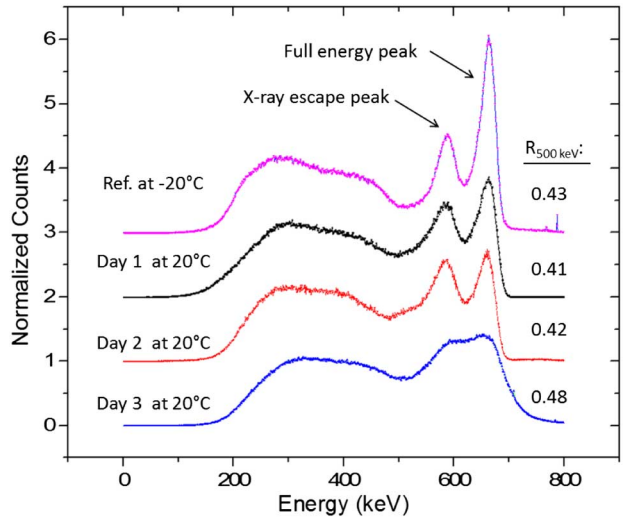

Fig. 2. Time evolution of the depth-corrected $^{137}\mathrm{Cs}$ energy spectrum for detector #44AB1R. Each spectra is from a 24-hour measurement. The spectrum at $-20°\mathrm{C}$ is shown for reference. Days 1-3 were taken at room-temperature. The spectra are offset for clarity.

C. Refabricated Detectors

After two of the detectors were polarized, RMD Inc. removed the electrodes along with 0.5 mm of bulk material under the anode and cathode surfaces. New Cr/Au electrodes were applied and the detectors were retested at $-20°\mathrm{C}$ and -1000 V cathode bias.

III. Results

A. Detector #44AB1R

After 15 days of room-temperature operation, detector #44AB1R suffered complete failure. Fig. 2 shows the time-dependent energy resolution degradation in the depth-corrected single-pixel-event $^{137}\mathrm{Cs}$ energy spectrum. After three days of continuous room-temperature operation, the photopeak and Tl characteristic x-ray escape peak are almost unresolvable. The spectra are normalized by the total number of counts which is not preserved from $-20°\mathrm{C}$ to room-temperature. The processing electronics are noisier at room temperature which causes noise triggers and increases the dead time of the system. The total number of counts for the reference spectrum and day 1, day 2, and day 3 of room temeprature operation were 2.8×10^6, 2.2×10^6, 2.1×10^6, and 2.0×10^6 respectively. The ratio of counts above 500 keV to total counts is listed to the right of each photopeak and remains relatively constant.

Fig. 3 shows the leakage current and average electron drift velocity over the first 300 hours of room-temperature operation. Both the leakage current and average electron drift velocity are indirect measurements of the average electric field, explaining

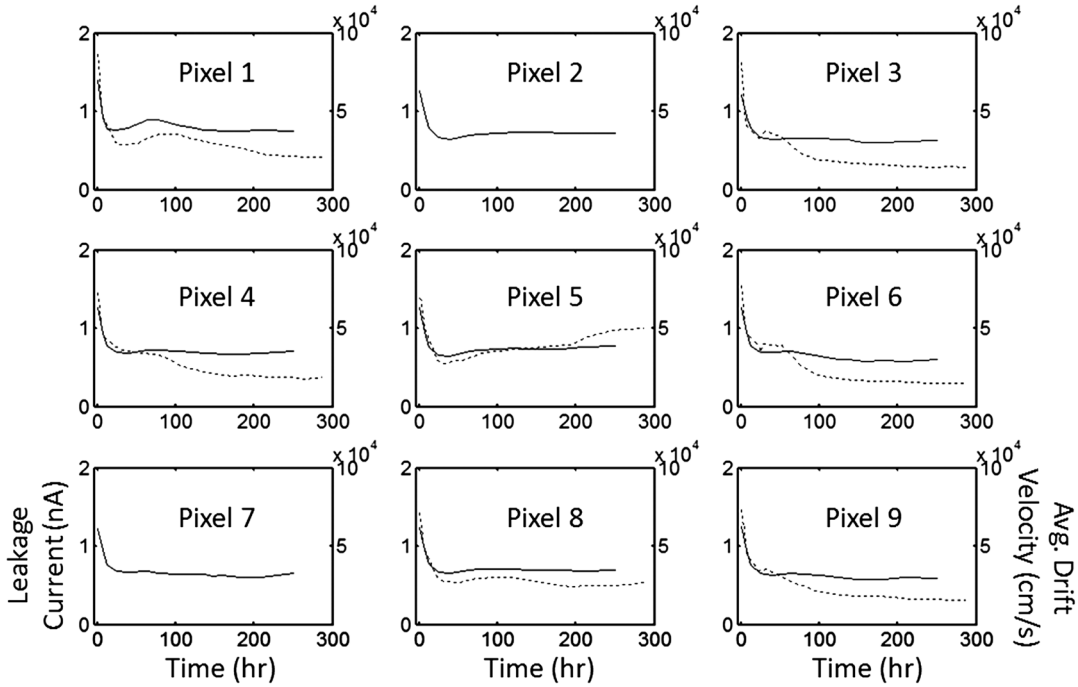

Fig. 3. Leakage current (dashed curve) and average electron drift velocity (solid curve) over the first 300 hours of room-temperature operation for detector #44AB1R. Both quantitates are indirect measurements of the effective electric field. Leakage current data were not available for pixels two and seven.

the observed correlation in Fig. 3. As the device polarizes, the decreasing electric field, possibly the result of ionic conduction, causes a reduction in both the leakage current and electron drift velocity. In all nine pixels, both quantities drop dramatically over the first twelve hours and then reach a horizontal asymptote, suggesting that most of the electric field reduction occurs at the beginning of room temperature operation.

From Fig. 2 and Fig. 3 no correlation exists between the average electric field and the detector performance. For example, the electric field decreases dramatically in the first 12 hours while the detector performance shows minimal change. Similarly, a dramatic decrease in energy resolution occurs between day two and day three, while there is little change in the electric field strength (hours 24 to 48 in Fig. 3).

While ionic conduction is likely causing a reduction in the electric field [9], [14], Fig. 2 and Fig. 3 show that this reduction is not causing the device degradation. The degradation is more likely the result of the Au atoms in the electrode diffusing into the bulk crystal creating sub band-gap trap centers, as outlined in [5].

In addition to poor energy resolution, the average raw ADC amplitude of the induced voltage pulses decreased as a function of time. The gamma-ray spectra were too poor to track the photopeak centroid after a few days (see Fig. 2) so alpha-particles from $^{241}\mathrm{Am}$ were used to quantify the ADC amplitude shift. Unlike gamma-rays, alpha-particles always deposit their full energy in a single interaction, so the anode alpha spectrum only contains a full-energy peak. Similarly, the cathode spectrum only contains a full-energy peak because the energy deposition occurs right at the cathode surface. Fig. 4 shows the normalized full-energy alpha-particle peak shift as a function of time for both the cathode and the anode signals in pixel eight.

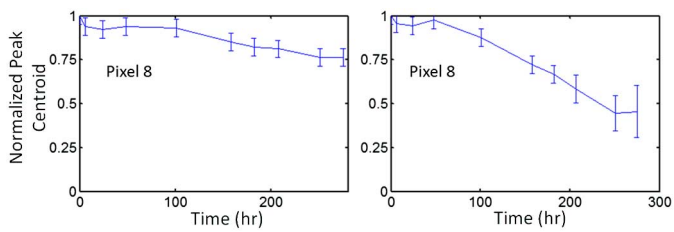

Fig. 4. Full energy alpha-particle peak centroid shift as a function of time for (a) the cathode and (b) the anode signals in detector #44AB1R.

Due to limited geometry, only the three center pixels (pixels two, five, and eight) had sufficient alpha data. Pixel 8 is representative of all three pixels. Fig. 4 shows that the anode peak shift is much greater than the cathode peak shift, indicating an increase in trapping over time.

According to the Shockley-Ramo Theorem, the induced charge on an electrode is proportional to the generated charge multiplied by the change in weighting potential [15], [16]. (Refer to Ref. [17] for a complete description of the Shockley-Ramo theorem as it applies to pixelated devices). The largest change in weighting potential for a pixelated anode (see Fig. 5(b)) occurs near the anode surface (i.e. most of the anode signal induction occurs at the end of the electron drift). Therefore, any increase in the number of trapping sites, either in the bulk or near the anode surface, will affect the anode signal more than the cathode signal. The discrepancy between the anode and cathode peak shifts as a function of time indicates an increase in the number of trapping sites, likely caused by the diffusion of Au into the crystal. Isolating bulk trapping effects from anode side trapping effects requires examining the time-dependent photopeak centroid as a function of depth. Due

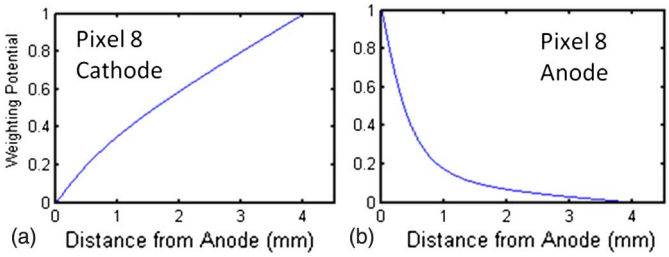

Fig. 5. (a) Cathode and (b) anode weighting potentials for detector #44AB1R. This detector is 4 mm thick.

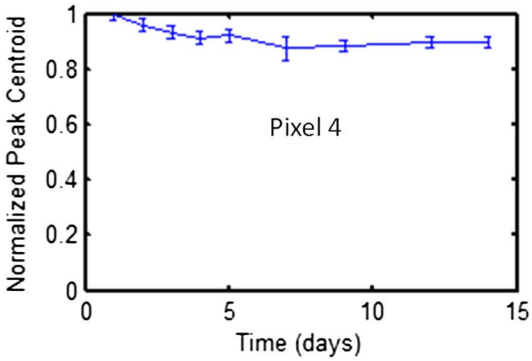

Fig. 6. Photopeak centroid as a function of time in pixel 4 of detector #935-29-AA1-3. The average degradation is representative of all 9 pixels.

to rapid spectroscopic performance degradation (see Fig. 2), this analysis could not be performed on detector #44AB1R.

B. Detector #935-29-AA1-3

Detector #935-29-AA1-3 achieved 2.06% FWHM at 662 keV at $-20°C$, which is about average for pixelated TlBr detectors tested at UM [10]. It polarized after 15 days of room-temperature operation. Due to geometric limitations, the alpha-particle efficiency was too low to track the ADC gain shift over time. However, the gamma-ray energy resolution was sufficient throughout polarization and Fig. 6 shows the photopeak centroid as a function of time for pixel 4. The slope of pixel 4 is 5.9×10^{-3} normalized ADC/day and is representative of the nine pixels. The average slope and standard deviation over the nine pixels is 6.0×10^{-3} and 2.3×10^{-3} normalized ADC/day respectively. From Fig. 4(b), the slope in pixel 8 for detector #44AB1R was 5×10^{-2} normalized ADC/day. The relatively high signal loss contributes to the poor energy resolution observed in detector #44AB1R.

Fig. 7 summarizes the time-dependent gamma-ray energy resolution during room-temperature operation. The energy resolution ranged from 4% to 9% FWHM at 662 keV. Similar to #44AB1R, there is no correlation between the average electric field strength (measured indirectly using the average drift velocity and leakage current) and the gamma-ray energy resolution for detector #935-29-AA1-3.

Fig. 8 shows the cathode waveforms in pixel seven from alpha particles incident on the cathode side of the detector after one day and eight days of room-temperature operation. Individual waveforms are shown in gray with the average waveform shown in black. Initially, the waveforms were uniform and showed

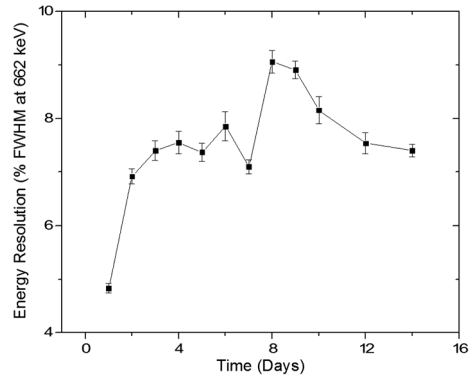

Fig. 7. Energy resolution as a function of time for detector #935-29-AA1-3.

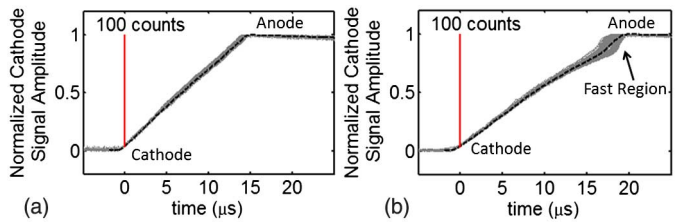

Fig. 8. Cathode waveforms of alpha-particles incident on the cathode side of detector #935-29-AA1-3 after (a) one day and (b) eight days of operation at room temperature. Data shown are from pixel seven but are representative of the entire detector.

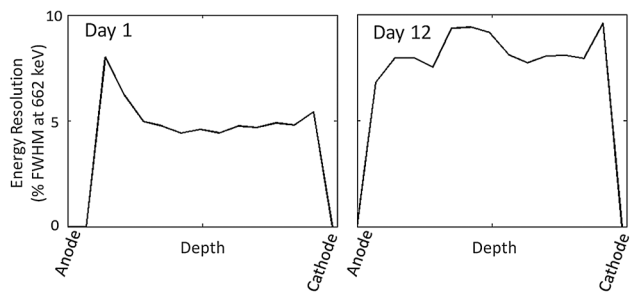

Fig. 9. ^{137}Cs depth separated energy resolution for #935-29-AA1-3 after (a) 1 day (b) 12 days of applied bias at room temperature. The uniform energy resolution degradation as a function of depth indicates an anode side polarization effect. Data shown are from pixel six but are representative of the entire detector.

little deviation from the average. During the eighth day, a fast region, evidenced by the steep slope, developed near the anode side. Additionally, the waveforms show a large deviation in this region. Fast regions near the anode surface have been observed in other 5 mm thick TlBr detectors [10]. The high drift velocity and deviation is likely caused by the non-uniform accumulation of negative space charge (the result of ionic conduction) near the anode electrode. According to Poisson's equation, negative space charge under the anode causes a larger electric field in the region of space charge and a lower electric field in the rest of the bulk. Fig. 8 indicates that the dominating polarization effects occur near the anode. If the polarization phenomena occurred throughout the bulk, there would be significant deviation through the whole waveform instead of just near the anode. Fig. 8 shows data for pixel seven but is representative of all pixels.

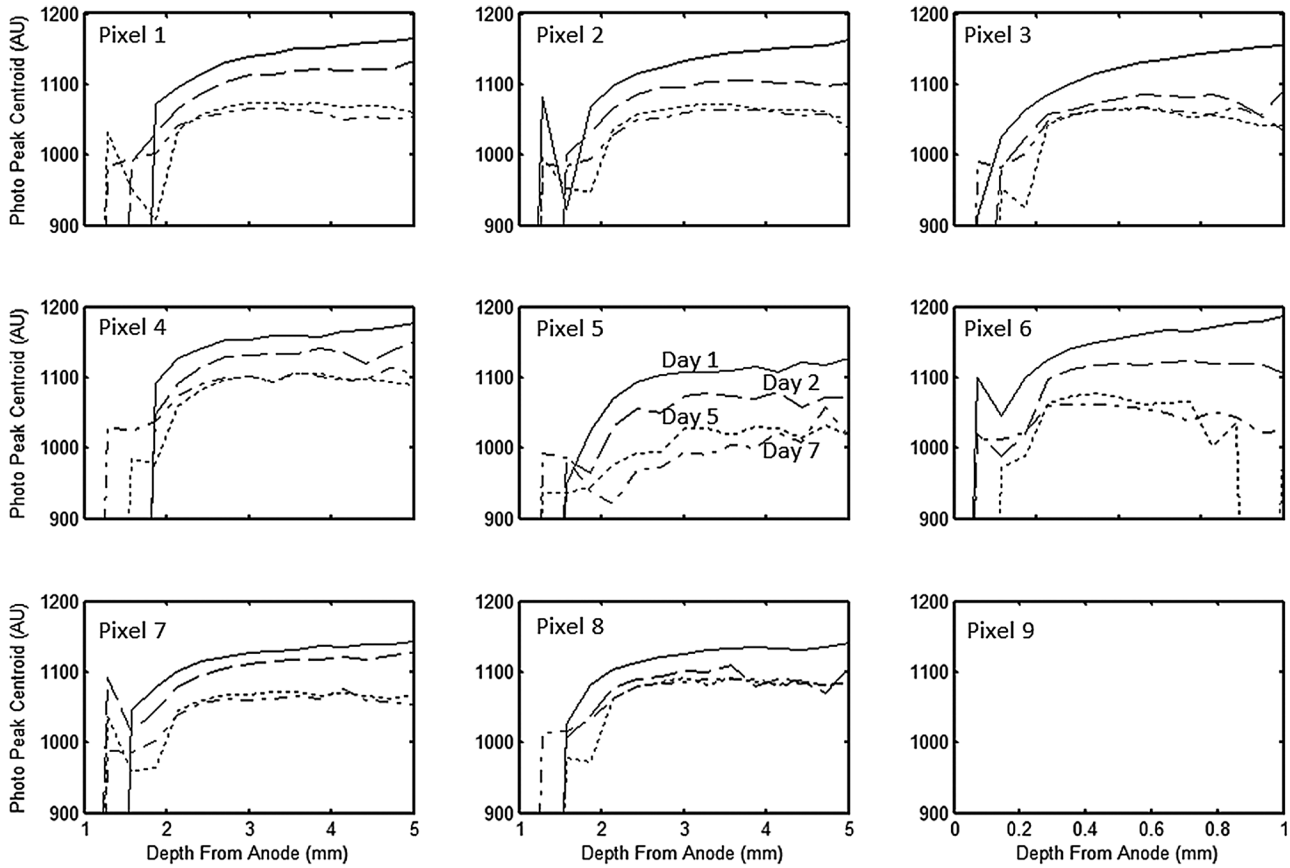

Fig. 10. Photopeak centroids as a function of depth during day 1 (solid curve), day 2 (dashed), day 5 (dotted) and day 7 (dashed-dotted) for detector #935-29-AA1-3. The photopeak amplitudes decreased uniformly at all depths, indicating that trapping sites were created near the anode surface.

Fig. 9, which shows depth-dependent energy resolution in pixel 6 for day one and day twelve, also indicates anode side degradation. If the polarization phenomenon affected the bulk, then the energy resolution would degrade more severely near the cathode surface. Instead, Fig. 9 shows a uniform degradation at all depths, indicating that polarization for this detector is concentrated near the anode surface.

Photopeak amplitude shifts were also observed in detector #935-29-AA1-3. The gamma spectroscopy remained good enough to observe the depth-dependent photopeak amplitude as a function of time during polarization (see Fig. 10). The average photopeak amplitude decreased with time, indicating the trapping site concentration increased. However, the photopeak amplitude decreases uniformly at all depths, suggesting that most of the new trapping sites are created near the anode surface. If new trapping sites were created in the bulk, the photopeak amplitudes near the cathode surface would decrease more rapidly than the photopeak amplitudes near the anode surface. Pixel 9 had insufficient counts at each depth so it should be ignored. The introduction of new trapping sites near the anode surface could be caused by the diffusion of Au from the electrode to the crystal [5]. It is likely that the space charge buildup from ionic conduction is necessary for the Au diffusion mechanisms outlined in Ref. [5] and Ref. [7]. Therefore, it is expected that both a fast region (the result of the ionic conduction) and heavy trapping (the result of Au diffusion) occur near the anode electrode.

C. Refabricated Detectors

Detectors #70BA1R and #44A12R operated at room-temperature for one and five days respectively. Fig. 11 shows the $^{137}\mathrm{Cs}$ gamma-ray spectrum after initial bias at $-20^{c}irc\mathrm{C}$, during polarization at room temperature, and after refabrication at $-20^{\circ}\mathrm{C}$. In both cases the energy resolution was the best during initial operation, worsened during polarization, and improved to almost initial values after refabrication. During the refabrication process 1 mm of material (20% of the bulk crystal) was removed. The anode weighting potential is significantly non-zero approximately one pixel pitch from the anode surface. Therefore, removing 20% of the material causes the poor spectroscopy region to become a larger fraction of the crystal bulk, resulting in slightly worse energy resolution after refabrication. Performance recovery following refabrication indicates that polarization does not permanently damage the bulk material but is localized to near the electrode surfaces.

IV. Conclusions

Polarization occurs in TlBr detectors after days to months of room temperature operation. By studying the leakage current, gamma-ray response, and alpha particle response of two TlBr detectors we conclude that the performance degradation is more heavily influenced by mechanisms occurring near the anode surface as opposed to near the cathode surface or in the bulk. By

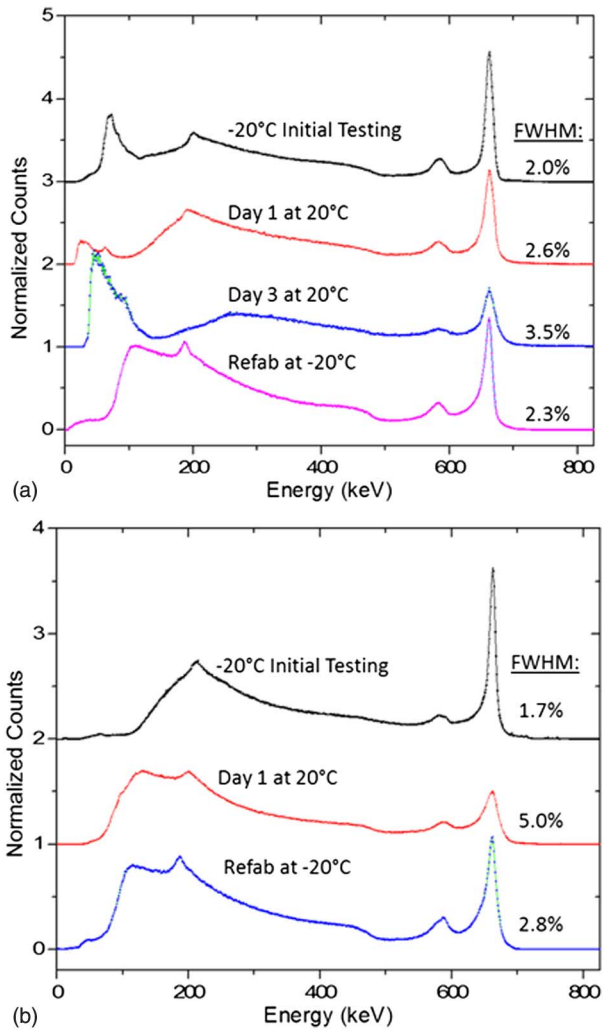

Fig. 11. Single-pixel, ^{137}Cs energy spectra for detectors (a) #44A12R and (b) #70BA1R after initial bias, during room temperature operation, and after refabrication.

observing the change in the depth-dependent photopeak amplitude over time, we conclude that trapping sites are formed near the anode, possibly the result of Au migration from the electrode into the crystal. By refabricating and retesting devices that have polarized at room temperature, we conclude that polarization does not permanently damage the bulk crystal but is localized to a thin layer (< 0.5 mm) near the electrode surfaces. Therefore, if long term stability of room temperature TlBr detectors is desired, future work should focus on improving the electrode design to minimize reactions between the surface TlBr and the contact material.

References

[1] T. Onodera, K. Hitomi, and T. Shoji, "Spectroscopic performance and long-term stability of thallium bromide radiation detectors," *Nucl. Instrum. Methods Phys. Res. A*, vol. 568, pp. 433–436, Jul. 2006.

[2] B. Donmenz, Z. He, H. Kim, L. J. Cirignano, and K. S. Shah, "The stability of TlBr detectors at low temperature," *Nucl. Instrum. Methods Phys. Res. A*, vol. 623, no. 3, pp. 1024–1029, 2010.

[3] K. Hitomi, Y. Kikuchi, T. Shoji, and K. Ishii, "Polarization phenomena in TlBr detectors," *Nucl. Instrum. Methods Phys. Res. A*, vol. 683, pp. 53–62, 2012.

[4] L. F. Voss, A. M. Conway, R. T. Graff, P. R. Beck, R. J. Nikolic, A. J. Nelson, S. A. Payne, H. Kim, L. L. Cirigano, and K. Shah, "Surface processing of TlBr for improved gamma spectroscopy," in *Proc. IEEE Nuclear Science Symp. Conf. Rec. (NSS/MIC)*, Oct. 30–Nov. 6 2010, pp. 3746–3748.

[5] A. Conway, L. Voss, A. Nelson, P. Beck, T. Laurence, R. Graff, R. Nikolic, S. Payne, H. Kim, L. Cirignano, and K. Shah, "Fabrication methodology of enhanced stability room temperature TlBr gamma detectors," *IEEE Trans. Nucl. Sci.*, vol. 60, no. 2, pp. 1231–1236, Apr. 2013.

[6] C. Thrall, W. Koehler, Z. He, H. Kim, L. Cirignano, and K. Shah, "Characterization of the polarization process in thallium-bromide detectors," presented at the IEEE RTSD, Anaheim, CA, USA, Oct, 2012.

[7] K. Hitomi, T. Shoji, and Y. Niizeki, "A method for suppressing polarization phenomena in TlBr detectors," *Nucl. Instrum. Methods Phys. Res. A*, vol. 585, pp. 102–104, Jan. 2008.

[8] V. Kozlov, M. Kemell, M. Vehkamaki, and M. Leskela, "Degradation effects in TlBr single crystals under prolonged bias voltage," *Nucl. Instrum. Methods Phys. Res. A*, vol. 576, pp. 10–14, Jun. 2007.

[9] K. Hitomi, Y. Kikuchi, T. Shoji, and K. Ishii, "Improvement of energy resolutions in TlBr detectors," *Nucl. Instrum. Methods Phys. Res. A*, vol. 601, pp. 112–115, Aug. 2009.

[10] C. Thrall, "Alternative wide-band-gap materials for gamma-ray spectroscopy," Ph. D. dissertation, Univ. Michigan, Ann Arbor, MI, USA, 2013.

[11] Z. He, W. Li, G. Knoll, D. Wehe, J. Berry, and C. Stahle, "3-d Position sensitive CdZnTe gamma-ray spectrometers," *Nucl. Instrum. Methods Phys. Res. A*, vol. 442, no. 13, pp. 173–198, 1999.

[12] J. C. Kim, W. R. Kaye, W. Wang, F. Zhang, and Z. He, "Impact of drift time variation on the Compton image from large-volume CdZnTe crystals," *Nucl. Instrum. Methods Phys. Res. A*, vol. 683, p. 5362, 2012.

[13] C. Thrall, W. Kaye, Z. He, H. Kim, L. Cirignano, and K. Shah, "Transient behavior in TlBr gamma-ray detectors and its analysis using 3-d position sensing," *IEEE Trans. Nucl. Sci.*, vol. 60, no. 2, pp. 1162–1167, Apr. 2013.

[14] S. R. Bishop, W. Higgins, G. Ciampi, A. Churilov, K. S. Shah, and H. L. Tuller, "The defect and transport properties of donor doped single crystal TlBr," *J. Electrochem. Soc.*, vol. 158, pp. J47–J51, 2011.

[15] W. Shockley, "Currents to conductors induced by a moving point charge," *J. Appl. Phys.*, pp. 635–636, 1938.

[16] S. Ramo, "Currents induced by electron motion," in *Proc. I.R.E.*, Sep. 1939, p. 584.

[17] Z. He, "Review of the Shockley-Ramo theorem and its application in semiconductor gamma-ray detectors," *Nucl. Instrum. Methods Phys. Res. A*, vol. 463, pp. 250–267, 2001.